ATMOSPHERIC PHASE DELAY ESTIMATION FROM MULTIPLE SAR INTERFEROMETRY MEASUREMENTS

Yo Fukushima [(1)]

[(1)]*DPRI, Kyoto Univ., Gokasho, Uji, 611-0011, Japan. Email: yofukushima@rcep.dpri.kyoto-u.ac.jp*

ABSTRACT

The phase observed by SAR interferograms generally contains stochastic fluctuations that result from radar signals propagating through disturbed troposphere and ionosphere. The present study focuses on estimation of such stochastic atmospheric phase signals. Since these signals are linearly related to the unwrapped InSAR phase values, they can be solved in a least-squares framework under certain assumptions and constraints. Under the assumption that the random phase delay signals are as simple as possible, this study adopts the minimum norm constraint. Synthetic test results are consistent with theoretical expectation such that the standard deviation of the residuals (true - estimated) is equal to the standard deviation of the random fluctuation divided by the number of used SAR images. Atmospheric phase correction based on the proposed method is applied to a stack of ALOS/PALSAR data acquired over Kinki district, western Japan, where quasi-steady displacements of a few cm/year is occurring because of the subducting Philippine Sea Plate. It is found that the atmospheric noise reduces to a level expected from the synthetic tests, but that the amount of reduction is not enough to extract the displacement signals.

1. INTRODUCTION

The radar signals used by the satellite radar systems are influenced by the conditions of the troposphere and ionosphere as they propagate (*e.g.*, Hanssen, 2001). More specifically, the transmitting microwave experiences negative phase delays in the ionosphere in a dispersive manner and positive phase delays in the troposphere. The purpose of this study is to estimate such atmospheric phase delay components from SAR interferograms.

2. METHOD

I start from a general system of observation equations of

$$\mathbf{d} = \mathbf{A}\mathbf{x} + \mathbf{e}\,, \qquad (1)$$

where the data vector $\mathbf{d} = [d_1, d_2, \ldots, d_N]^T$ is composed of N unwrapped InSAR observations, the model vector $\mathbf{x} = [\mathbf{a}, \mathbf{u}]^T = [a_1, a_2, \ldots, a_N\ u_1, u_2, \ldots, u_N]^T$ is composed of the atmospheric and orbital residual signals, **a**, and the line-of-sight (LOS) displacements with respect to the first date of acquisition in N-1 epochs, **u**. The design matrix **A** relates the data and model vectors, and the error vector **e** results from thermal noise, decorrelation, etc (Fig. 1). The rank of the design matrix is, at best, N-1, whereas the number of model parameters is 2N-1. Eq. (1) holds for every pixel in a stack of unwrapped interferograms.

Let us further assume that the displacement signals are much smaller than the atmospheric delay signals, so that

$$\mathbf{d} = \mathbf{G}\mathbf{a} + \mathbf{e}\,, \qquad (2)$$

then the number of unknowns reduces to N. This assumption, that the atmospheric signals are much larger than the deformation signals, is in fact applicable in most occasions. I further assume that the orbital residual signals due to orbit inaccuracies are negligibly small, which is reasonable for modern satellites such as ENVISAT or ALOS.

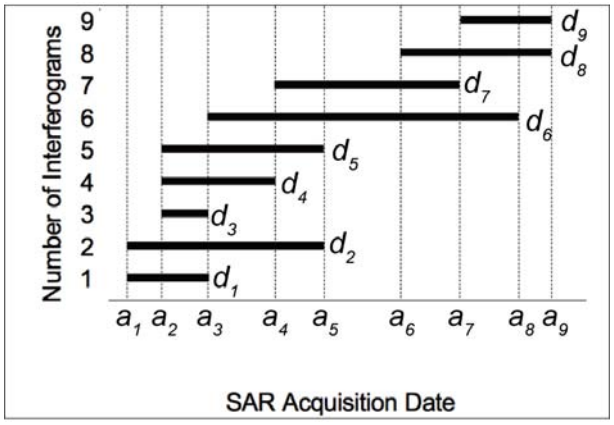

Figure 1. Schematic figure explaining the data and model parameters. The data vector is composed of unwrapped interferometric phase (d_1, d_2, *…). Each acquisition is associated with atmospheric and orbital residual phase (*a_1, a_2, *…). The orbital phase is neglected in this study.*

The rand of the design matrix **G** is, at best, N-1, hence we need additional constraints to solve Eq. (2). We have different options; for example, if we have a priori information such that the state of the atmosphere was quiet on a certain day, then we can fix the delay to be zero on that day. Alternatively, we can adopt the minimum norm solution of Eq. (2), based on an

Proc. 'Fringe 2011 Workshop', Frascati, Italy,
19–23 September 2011 (ESA SP-697, January 2012)

expectation that the random phase delay signals are simple. The minimum norm strategy is exploited in detail in the followings.

3. SYNTHETIC TESTS

I first created synthetic data sets in the following way. I modeled the atmospheric phase delays as randomly correlated fluctuation. The autocorrelation function that characterizes the statistical property is assumed to be exponential (but can be another type), and the frequency distribution of the phase delays is assumed to be Gaussian. Note that since we are to solve Eq. (2) in a least square's scheme, the phase delays should have a Gaussian distribution. This is usually met in reality (Fukushima *et al.*, 2005). Different phase delays are simulated for each SAR acquisition, and synthetic interferograms (differential phase values) are created by subtracting phase values in one image from those in another. Lastly, the minimum norm solutions are obtained on pixel-by-pixel basis.

This test was run for different numbers of used SAR images. Fig. 2 shows the results for N = 2, 3, 4 and 10. In each subset the assumed and estimated delays are shown. By nature of the method, the two images of estimated solutions for N = 2 have an identical pattern having opposite signs (Fig. 2, N = 2, bottom). By running this kind of simulations many times, it is found that the standard deviation of the residuals (true – estimation) decreases with √N (Fig. 3).

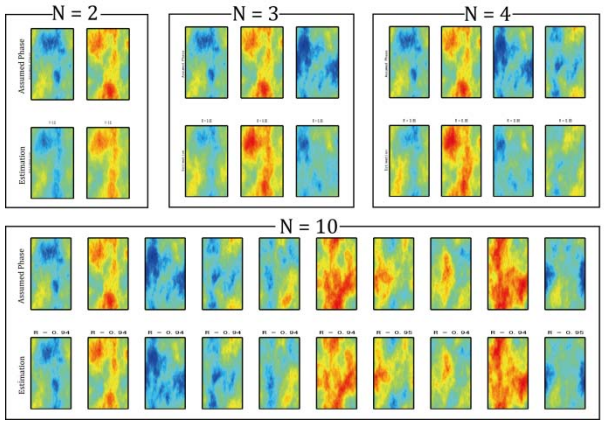

Figure 2. Results of synthetic tests for N=2, 3, 4 and 10. The upper row for each subset shows the true model that corresponds to atmospheric phase delay. The bottom row shows the estimation. Color shows the amplitude of the signal whose scale is arbitrary.

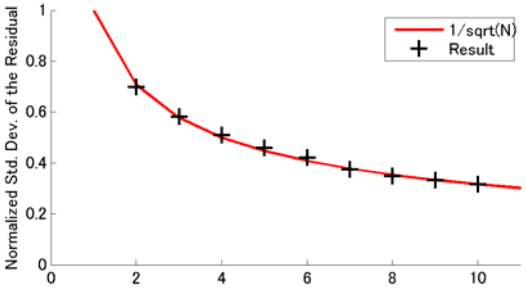

Figure 3. The normalized standard deviation of the residual (true – estimation) is obtained for different number of used SAR images (plus signs) and compared with the theoretical expectation such that the standard deviation decreases with the squared root of the number of used images (red curve).

The decrease of the residuals as N increases is expected from simple analytic considerations. For simplicity I ignore the noise term **e** in Eq. (2). Note that the noise is also not assumed in the test. Adding the noise only results in additional uncorrelated white-type noise and does not affect the conclusion given below. Without the noise,

$$\begin{aligned} \mathbf{d} &= \mathbf{G}\mathbf{a} \\ &= \mathbf{G}\mathbf{a}^{true} \\ &= \mathbf{G}\mathbf{a}^{est} . \end{aligned} \qquad (3)$$

Here, the superscripts *true* and *est* correspond to true and estimated models, respectively. The second equality holds because the problem is underdetermined. The minimum norm solution $\mathbf{a}^{est}$ can be expressed as

$$\begin{aligned} \mathbf{a}^{est} &= [\mathbf{G}^{\mathrm{T}}\mathbf{G}\mathbf{G}]^{-1}\mathbf{d} \\ &= [\mathbf{G}^{\mathrm{T}}\mathbf{G}\mathbf{G}]^{-1}\mathbf{G}\mathbf{a}^{true} \\ &= \mathbf{R}\mathbf{a}^{true} . \end{aligned} \qquad (4)$$

where **R** is the resolution matrix. The resisudal $\mathbf{da}^{est}$ is then

$$\begin{aligned} \mathbf{da}^{est} &= \mathbf{a}^{true} - \mathbf{a}^{est} \\ &= (\mathbf{I} - \mathbf{R})\,\mathbf{a}^{true} . \end{aligned} \qquad (5)$$

After some simple calculations, it can be found that

$$\mathbf{I} - \mathbf{R} = \frac{1}{N}\begin{bmatrix} 1 & \cdots & 1 \\ \vdots & \ddots & \vdots \\ 1 & \cdots & 1 \end{bmatrix} . \qquad (6)$$

Eqs. (5) and (6) indicate that the residual vectors for all the images are identical and equal to the mean of the true atmospheric signals:

$$da_1 = da_2 = \cdots = da_N = \text{mean}(\mathbf{a}^{true}). \quad (7)$$

Therefore, if the atmospheric signals has a normal distribution as assumed in the synthetic test, i.e., $\mathbf{a}^{\text{true}} \sim N(0, \sigma^2)$, then the residuals also have a normal distribution and the variance becomes that of the true signal divided by the number of images, i.e., $\mathbf{da}^{\text{true}} \sim N(0, \sigma^2/N)$. Fig. 3 shows that this theoretical expectation is consistent with the simulation results.

4. APPLICATION TO ALOS/PALSAR DATA ACQUIRED OVER WESTERN JAPAN

The proposed method is applied to ALOS/PALSAR data acquired over Kinki district, western Japan (Fig. 4). A total of 15 images are used (Table 1). In this region, the Phillipine Sea Plate subducts under the Amurian Plate on which the Japanese islands are located. The plate interface is locked at seismogenic depths, causing a few centimeters of steady displacements.

In the followings, the method proposed in Section 2 is applied to two subsets: 1) 6 images acquired between July 2007 and May 2008, and 2) 9 images acquired between Oct. 2009 and Oct. 2010. The purpose is to estimate the atmospheric signals in each subset and remove from interferograms, and then try to detect the secular deformation using corrected interferograms. The time spans of the two subsets are 10.5 and 12 months, respectively. The displacements that occurred within each time span are neglected.

The processing procedure is as follows:

1) Compute and unwrap small-baseline interferograms (Fig. 5, Table 2),
2) Estimate the atmospheric components in each subset independently,
3) Subtract the estimated atmospheric components from the original,
4) Compute the ground motion from long temporal-baseline (inter-subset) interferograms,

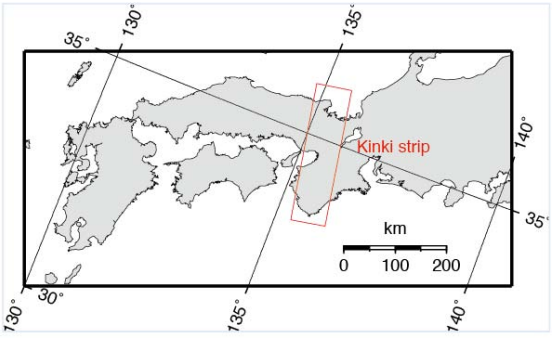

Figure 4. Map of southwest Japan with the analyzed strip indicated by red triangle.

1st subset		2nd subset	
1:	20070711	7:	20091016
2:	20070826	8:	20091201
3:	20071011	9:	20100116
4:	20080111	10:	20100303
5:	20080226	11:	20100418
6:	20080528	12:	20100603
		13:	20100719
		14:	20100903
		15:	20101019

Table 1. Acquisition dates of the data used in this study, shown in yyyymmdd format. The first and second columns correspond to the two subsets within which the atmospheric signals are estimated independently.

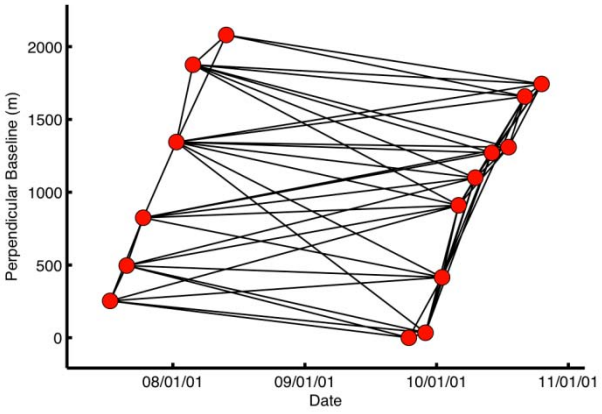

Figure 5. Acquisition dates and perpendicular baseline for the Kinki data set. Red circles indicate the SAR acquisitions and black lines indicate the interferometric pairs.

Fig. 6 shows the original unwrapped interferograms that were processed in this study. From these, atmospheric signals were estimated in the two subsets independently (Figs. 7 and 8). On some days (e.g., May 2008 and Oct. 2010), large fluctuations of more than 0.3 meters can be recognized, whereas some other days were quiet (e.g., Jan. 2008). Next, the estimated atmospheric signals were subtracted from the original to produce corrected interferograms (Fig. 9). The signals in the interferograms of short temporal baselines are suppressed essentially because I assumed no deformation within the time span of each subset. Other interferograms

where color variation is recognized correspond to long temporal-baseline paris. The mean velocity was then obtained from stacking of the long-term interferograms (Fig. 10). It is obvious from comparison with expectation from GPS displacements that the estimated mean velocity still contains significant atmospheric signals. Nevertheless, the amount of atmospheric contribution is greatly reduced. Indeed, we expect from the number of used images that the noise be reduced roughly by 1/2 to 1/3 (Fig. 3), which appears to be met in the result. In order to further increase the deformation detection capability, this method should be combined with other manipulations such as removal of interferograms heavily affected by atmospheric disturbances or estimation of atmospheric phase screens using numerical modeling.

5. CONCLUSIONS

In many cases atmospheric phase delay signals are much larger than ground movement signals. I showed that it is possible to extract atmospheric signals when displacement signals are negligible. Through synthetic tests the minimum norm method was shown to be able to estimate the atmospheric phase delay, with the standard deviation of the residual proportional to the squared root of the number of used images.

From application to ALOS/PALSAR data acquired over Kinki district, western Japan, it was found that the atmospheric signals could be estimated and removed from interferograms to increase the detection capability of the ground deformation but also that the direct application of the method was not sufficient for the purpose of deformation signal detection for the particular target.

The present study is at least useful for studies on the troposphere and ionosphere since the proposed method directly provides the phase delay maps in high spatial resolution. The idea of this method may also be useful to remove atmospheric signals in order to improve the capability of detecting ground deformation signals.

REFERENCES

Fukushima, Y., V. Cayol and P. Durand, Finding realistic dike models from interferometric synthetic aperture radar data: The February 2000 eruption at Piton de la Fournaise, *J. Geophys. Res.,* **110**, B03206, doi:10.1029/2004JB003268, 2005.

Hanssen, R., *Radar Interferometry: Data Interpretation and Error Analysis*, Kluwer Academic Pub., 2001.

1: 20070711 – 20070826	21: 20080111 – 20091201	41: 20091201 – 20100303
2: 20070711 – 20071011	22: 20080111 – 20100116	42: 20091201 – 20100418
3: 20070711 – 20091016	23: 20080111 – 20100303	43: 20091201 – 20100603
4: 20070711 – 20091201	24: 20080111 – 20100418	44: 20100116 – 20100303
5: 20070711 – 20100116	25: 20080111 – 20100603	45: 20100116 – 20100418
6: 20070711 – 20100303	26: 20080111 – 20100719	46: 20100116 – 20100603
7: 20070826 – 20071011	27: 20080111 – 20100903	47: 20100116 – 20100903
8: 20070826 – 20091016	28: 20080111 – 20101019	48: 20100303 – 20100418
9: 20070826 – 20091201	29: 20080226 – 20080528	49: 20100303 – 20100603
10: 20070826 – 20100116	30: 20080226 – 20100303	50: 20100303 – 20100719
11: 20070826 – 20100303	31: 20080226 – 20100418	51: 20100303 – 20100903
12: 20070826 – 20100418	32: 20080226 – 20100603	52: 20100418 – 20100603
13: 20071011 – 20080111	33: 20080226 – 20100719	53: 20100418 – 20100719
14: 20071011 – 20100116	34: 20080226 – 20100903	54: 20100418 – 20101019
15: 20071011 – 20100303	35: 20080226 – 20101019	55: 20100603 – 20100719
16: 20071011 – 20100418	36: 20080528 – 20100903	56: 20100603 – 20100903
17: 20071011 – 20100603	37: 20080528 – 20101019	57: 20100603 – 20101019
18: 20071011 – 20100719	38: 20091016 – 20091201	58: 20100719 – 20100903
19: 20080111 – 20080226	39: 20091016 – 20100116	59: 20100719 – 20101019
20: 20080111 – 20080528	40: 20091201 – 20100116	60: 20100903 – 20101019

Table 2. List of interferometric pairs processed in this study. The date format is yyyymmdd. The numbering of 1 to 60 is the same for Figs. 6 and 9.

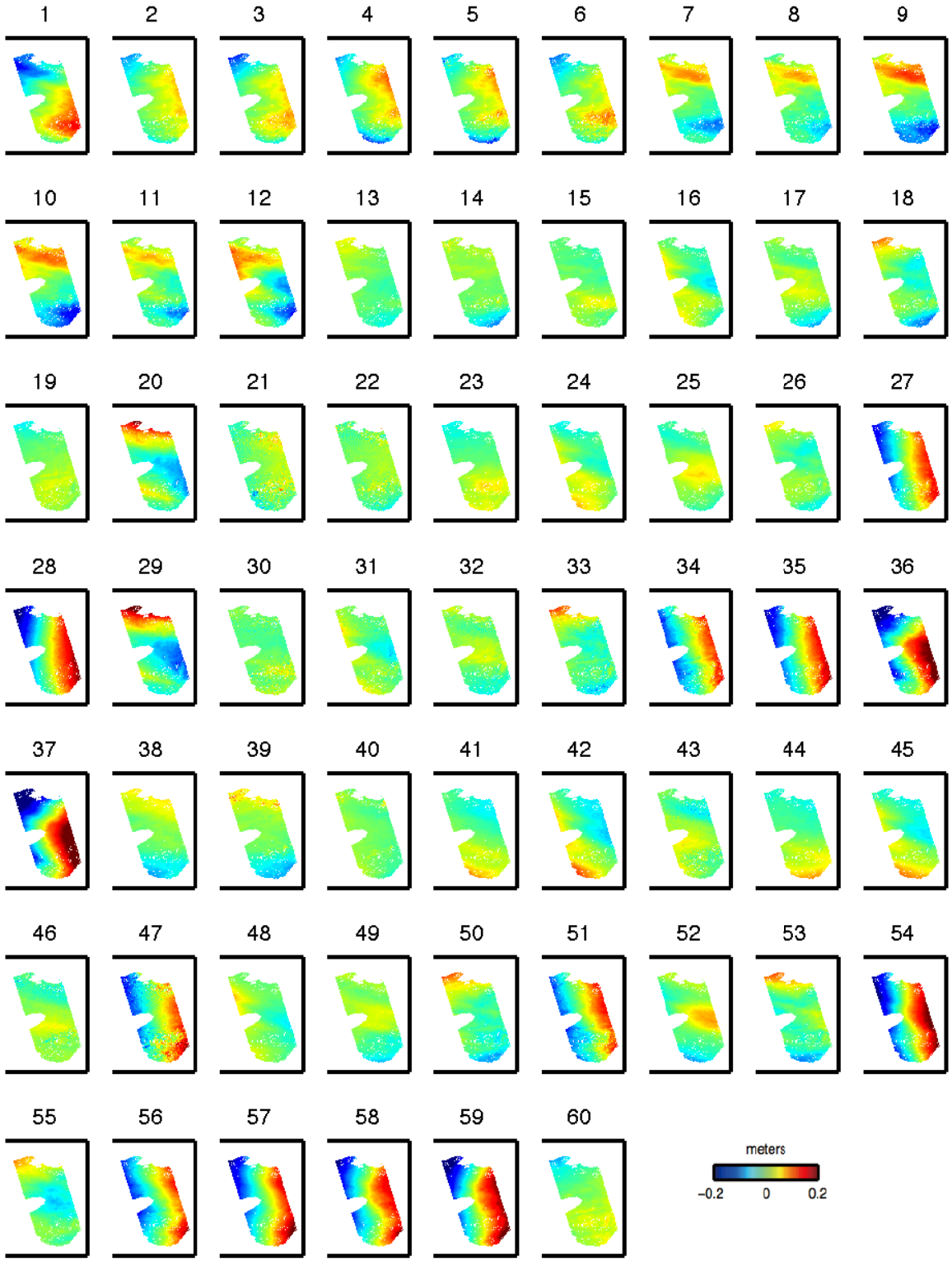

Figure 6. Unwrapped interferograms processed in this study. The color of blue to red corresponds to -0.2 to 0.2 meters of LOS displacements. See Table 2 for the master and slave dates of the 60 pairs.

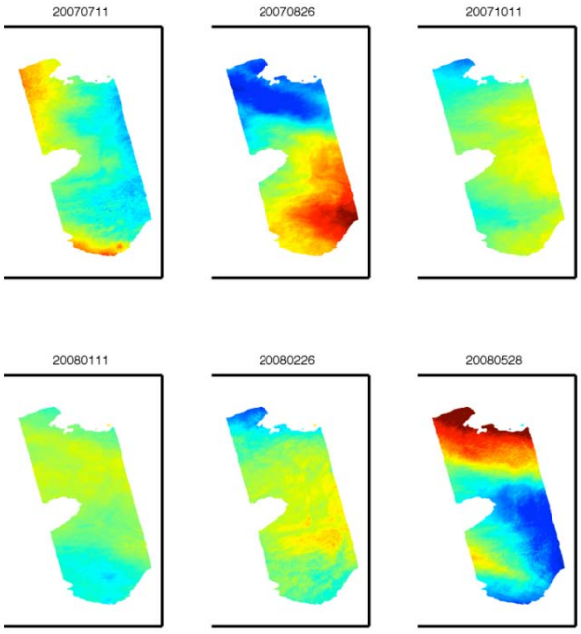

Figure 7. Atmospheric signals estimated for the first subset. Blue to red colors are equivalent to -0.2 to 0.2 meters of line-of-sight displacements.

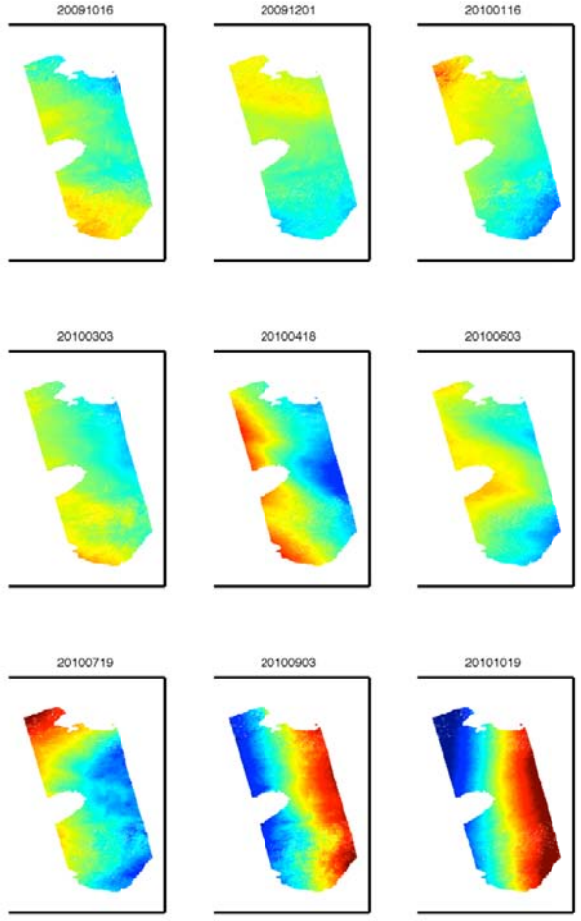

Figure 8. Same as Fig. 7, for the second subset.

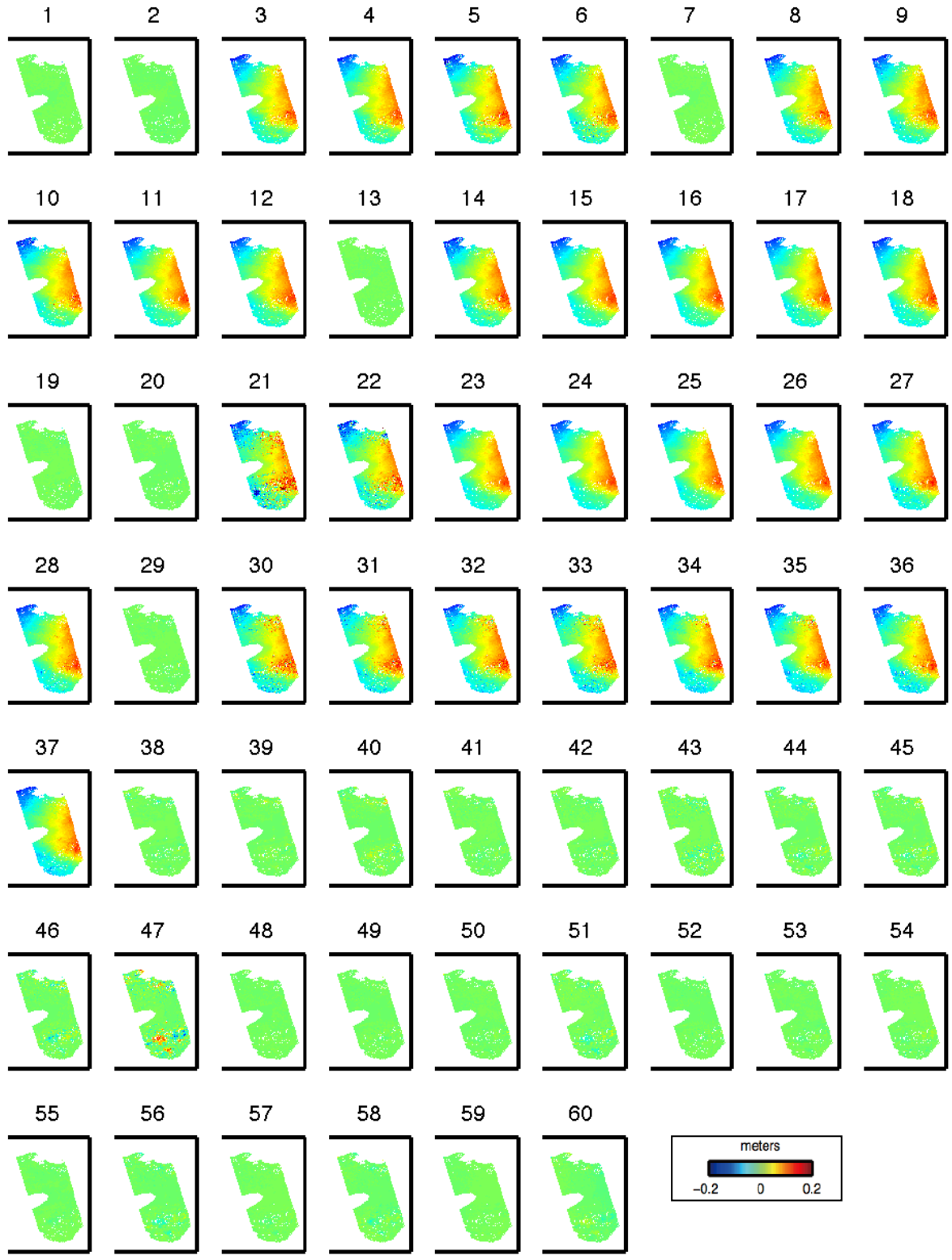

Figure 9. Unwrapped interferograms corrected for the atmospheric phase delays. The color of blue to red corresponds to -0.2 to 0.2 meters of LOS displacements.

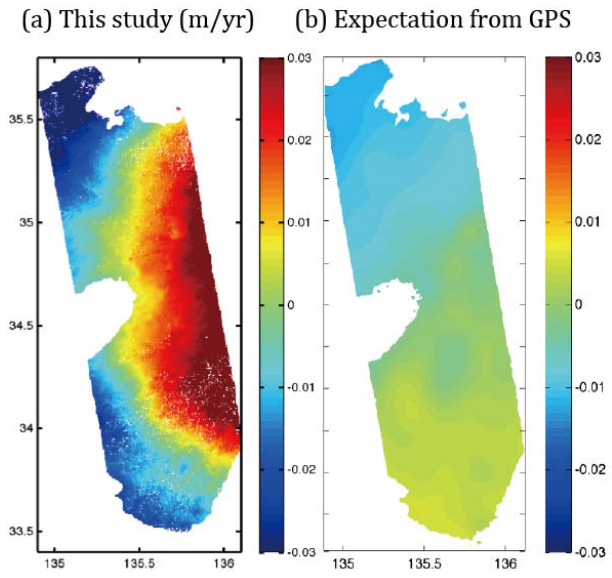

Figure 10. (a) Mean velocity obtained from atmosphere-corrected interferograms. (b) LOS velocity expected from GPS displacements, obtained by interpolating the GPS displacements recorded at stations distributed every 20-25 km.